Available online at www.sciencedirect.com
SCIENCE DIRECT®
Journal of Crystal Growth 256 (2003) 96–102
JOURNAL OF CRYSTAL GROWTH
www.elsevier.com/locate/jcrysgro

Difference of luminescent properties between strained InAsP/InP and strain-compensated InAsP/InGaAsP MQWs

H.P. Lei[a], H.Z. Wu[a,*], Y.F. Lao[a], M. Qi[a], A.Z. Li[a], W.Z. Shen[b]

[a] *State Key Laboratory of Functional Materials for Informatics, Shanghai Institute of Microsystem and Information Technology, Chinese Academy of Sciences, 865 Changning Road, Shanghai 200050, China*

[b] *Laboratory of Condensed Matter Spectroscopy and Opto-Electronic Physics, Department of Physics, Shanghai Jiao Tong University, Shanghai 200030, People's Republic of China*

Received 24 April 2003; accepted 6 May 2003
Communicated by Dr. M. Schieber

Abstract

Strained $InAs_{0.43}P_{0.57}/InP$ and strain-compensated $InAs_{0.43}P_{0.57}/In_{0.7}Ga_{0.3}As_{0.43}P_{0.57}$ multiple quantum well (MQW) structures were grown by gas source molecular beam epitaxy. The observations of up to 5 satellite-diffraction peaks from the high-resolution X-ray diffraction measurements demonstrate good crystalline quality for both structures. The temperature dependence of the 1e–1hh transition energies, the line width of photoluminescence (PL) spectra and emission efficiency η of the two quantum well structures are compared by low-temperature PL measurements. The temperature dependence of the 1e–1hh transitions of the two quantum well structures is similar to that of $InAs_{0.43}P_{0.57}$ bulk material. The thermal activation energies obtained for strain-compensated MQW are larger than those obtained for the strained one. Consequently, the PL emission efficiency decays much slower for the strain-compensated MQW than that for the strained one when temperature increases, indicating the superior temperature stability of luminescent efficiency for the strain-compensated MQW. The obtained results can be used as references to the design and fabrication of optoelectronic devices.

PACS: 68.65.+g; 78.55.−m; 63.20.kr; 78.60.−b

Keywords: A1. Emission efficiency; A1. Phonon–electron interaction; A1. Photoluminescence; A3. Strained and strain-compensated multi quantum wells

1. Introduction

In last decade, InAsP/InP heterostructures have been widely used as active layers of 1.3–1.55 μm laser diodes [1–4]. The realization of multiple quantum well (MQW) with strained layers improves the properties of quantum well lasers [3–5]. However, the critical thickness inherent in strained InAsP/InP MQWs limits the maximum number of QW growths. Recently, alternated compressive/tensile InAsP/InGaAsP MQWs have overcome the problem associated with the relaxation of strained layers. Meanwhile the strain-compensated

*Corresponding author.
E-mail address: hzwu@mail.sim.ac.cn (H.Z. Wu).

0022-0248/03/$ - see front matter
doi:10.1016/S0022-0248(03)01345-9

heterostructures also offer the advantage whereby the lineups of electron and hole bands can be shifted by the strain, giving an added flexibility in the design of optoelectronic devices [6–9]. However, the comparison of the difference in the luminescent properties between strained and strain-compensated InAsP/InGaAsP MQWs has not been investigated. For example, how much of quantum efficiency and of performance of strain-compensated laser diodes can be improved compared with the strained one. The underlying physics of the difference in the luminescent properties between strained and strain-compensated InAsP/InGaAsP MQWs is still not well studied. In this paper, samples with strained InAsP/InP and strain-compensated InAsP/InGaAsP MQWs were grown by gas source molecular beam epitaxy (GSMBE). Measurements of high-resolution X-ray diffraction (HRXRD) and low-temperature photoluminescence (PL) were carried out. The difference of luminescent properties between strained InAsP/InP and strain-compensated InAsP/InGaAsP MQWs are compared and studied semi-quantitatively.

2. Experiments

Both strained and strain-compensated InAsP/InGaAsP MQW structures were grown by gas source molecular beam epitaxy (GSMBE, V80). Ga and In vapors were obtained by heating the crucibles, As_2 and P_2 were obtained by cracking the AsH_3 and PH_3 gas when the gases flowed along the cracker which was set at 1000°C. The (0 0 1) oriented InP was used as substrates. Before the growth of QW layers an InP buffer, about 200 nm was firstly grown on the thermally cleaned InP substrate. For the strained sample A, 6-pair $InAs_{0.43}P_{0.57}$/InP MQWs with well width of 6 nm and barrier layer of 10 nm were followed. For the strain-compensated sample B, 6-pair $InAs_{0.43}P_{0.57}$/$In_{0.7}Ga_{0.3}As_{0.43}P_{0.57}$ MQWs with well width of 6 nm and barrier layer of 10 nm were followed, sandwiched by two cladding layers of $In_{0.7}Ga_{0.3}As_{0.43}P_{0.57}$. Finally, both samples were covered by an InP capping layer. The compressive strain of the well layer of $InAs_{0.43}P_{0.57}$ in sample A is 1.4%. The net strain in sample B is −0.09% [10].

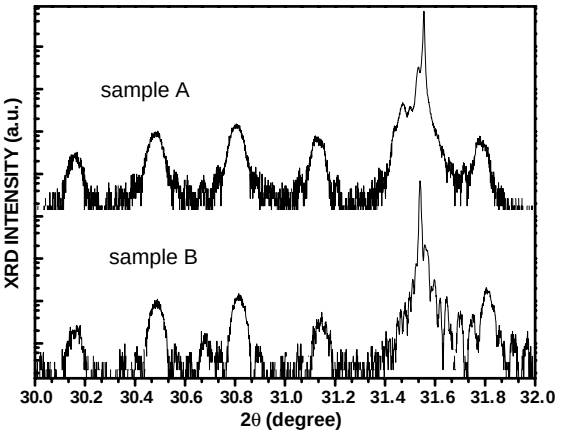

Fig. 1. High-resolution XRD profiles of samples A and B. Up to 5 satellite-diffraction peaks are observed, indicating the good period reproducibility of the heterostructures and the high crystalline quality.

The HRXRD measurements are shown in Fig. 1. Up to 5 satellite-diffraction peaks are observed clearly for both samples A and B. Although each sample has only 6 QWs the diffraction intensity of the satellite peaks are strong, which implies the good control of growth with both the thickness and layer compositions and the high crystalline quality of the samples. The periods of the MQW measured by the spacing between the satellite peaks are 15.6 and 15.5 nm for samples A and B, respectively. The PL measurements were taken using a NICOLET 860 Fourier transform IR spectrometer with a liquid nitrogen cooled InSb detector, and the resolution was of $2\,cm^{-1}$. The 514.5 nm line from an Ar^+ laser was used for cw excitation, and the excitation power was varied from 5 to 150 mW. The two samples were simultaneously mounted on the cold finger of the APD cryogenics system, and the temperature range was varied from 8 to 300 K.

3. Results and discussions

The PL spectra measured from the strained and strain-compensated samples are dominated by the recombination between $n = 1$ electron sub-band

and $n = 1$ heavy-hole sub-band (1e–1hh), either at low temperature or at room temperature, which are shown in Fig. 2. By the theoretical approximation of the transfer-matrix algorithm based on the Luttinger-Kohn Hamiltonian [11,12], the 1e–1hh transition energies are calculated to be 0.987 eV for sample A and 0.933 eV for sample B at room temperature. The calculated results are in good agreement with the measured PL peak energies.

At low temperature, the dependence of the integrated PL intensity (I_{PL}) of both samples on the excitation intensity (I_{ex}) has the form of $I_{pL} \propto I_{ex}^{\alpha}$ with $\alpha = 1.0 \pm 0.1 (T \leqslant 100\,K)$ for sample A and $\alpha = 1.00 \pm 0.03$ ($T \leqslant 150\,K$) for sample B, which reveals the excitonic radiative recombination being the prevailing recombination process in the low-temperature range [13].

Fig. 3 shows the variation of PL peak energy versus temperature. The curves (a) and (b) are the experimental results of the samples A and B, respectively. The curve (c) is obtained by Varshni Model [14] for the InAsP bulk material:

$$Eg^{InAs_xP_{1-x}}(T,x) = \left(Eg_0^{InAs} - \frac{\alpha_{InAs}T^2}{\beta_{InAs}+T}\right)x + \left(Eg_0^{InP} - \frac{\alpha_{InP}T^2}{\beta_{InP}+T}\right)(1-x) + Cgx(1-x), \quad (1)$$

where $Eg_0^{InAs} = 0.420\,eV$ and $Eg_0^{InP} = 1.421\,eV$ are InAs, InP band gap at lattice temperature of $T = 0\,K$. α_{InAs}, β_{InAs} are InAs temperature coefficients, $2.5 \times 10^{-4}\,eV/K$ and 75 K, respectively [15,16]. α_{InP}, β_{InP} are InP temperature coefficients, $3.63 \times 10^{-4}\,eV/K$ and 162 K, respectively [17]. The curve bowing parameter Cg is $-0.32\,eV$ [18]. Comparing the curves (a)–(c), we can see that the temperature dependences of sub-band energy levels for both samples have variation similar to the band gap of bulk $InAs_{0.43}P_{0.57}$. The blue shifts of curves (a) and (b) relative to curve (c) mainly originate from the quantum size effect of the

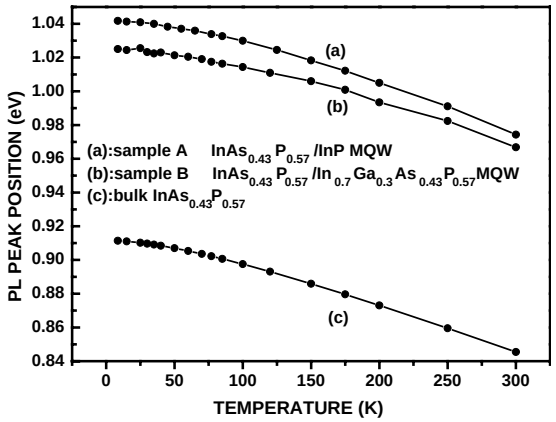

Fig. 3. Temperature dependence of the optical transition energy (1e–1hh). Curves (a) and (b) are the experiment results for sample A (strained $InAs_{0.43}P_{0.57}$/InP MQW) and sample B (strain-compensated $InAs_{0.43}P_{0.57}/In_{0.7}Ga_{0.3}As_{0.43}P_{.057}$ MQW). Curve (c) is calculation of band gap for bulk $InAs_{0.43}P_{0.57}$ by the Varshni Model.

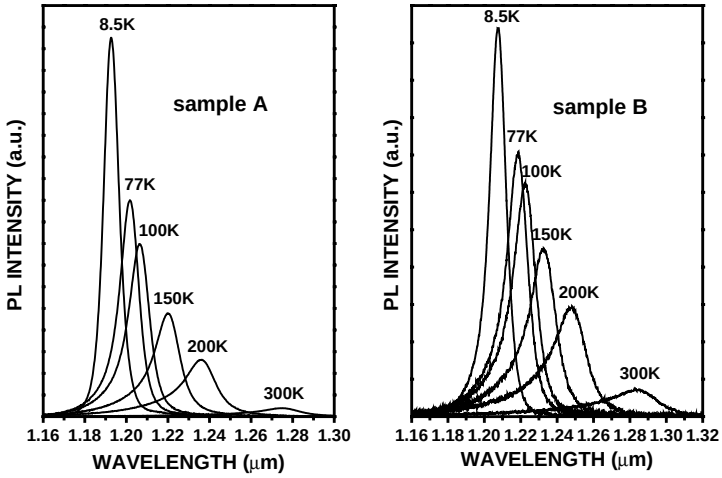

Fig. 2. PL spectra of samples A and B at the temperatures of 8.5, 77, 100, 150, 200, and 300 K.

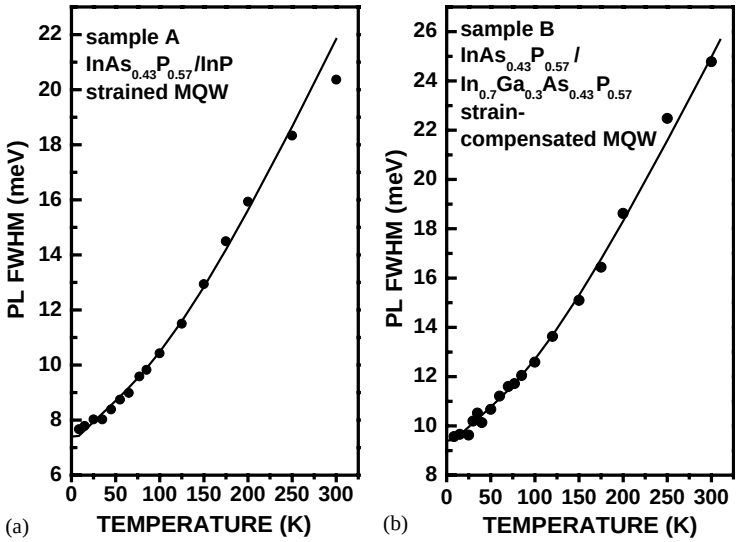

Fig. 4. Temperature dependence of the line width of PL spectra. The solid circles are the experiment data and the solid curves are the results fitted by Eq. (2): (a) for sample A and (b) for sample B.

quantum wells. The small difference of the optical transition energy between samples A and B results from different strains involved in the two samples. If we move curves (a) and (b) along the vertical coordinate and make it overlap curve (c) in the high temperature region, then, the measured peak energies of samples A and B deviate from curve (c) in the low-temperature region, 2.6 meV for sample A, and 7.7 meV for sample B. The energy shift may result from the localization of excitons in the potential well induced by the defects at hetero-interface and alloy composition fluctuation.

The temperature dependence of the full-width at half-maximum (FWHM) of PL spectra is a widely used method to study luminescent properties. As is well known, the measured exciton line shape is a convolution of an inhomogeneous factor and a temperature-dependent homogeneous factor. The inhomogeneous line width in MQW is mainly due to well width fluctuations, alloy disorder, compositional fluctuation in wells and barriers, and the hetero-interface roughness [19]. The homogeneous part can be attributed to the scattering between phonons and excitons, the carrier life broadening [19], and the interaction of carriers and excitons [20]. The contribution of the last two factors is negligible because the carrier life broadening is estimated to be 0.01 meV for InGaAsP/InGaAsP quantum well [19], and broadening due to the interaction of carriers and excitons is approximately 0.12 meV for GaAs quantum well ($T < 300$ K, and carrier density $n_0 \approx 10^{14}\,\mathrm{cm}^{-3}$) [20]. So, the homogeneous part is mainly determined by exciton scattering with acoustic and LO phonons. The temperature dependence of line width factor can be described by the exciton–phonon coupling model [20]

$$\Gamma = \Gamma_{\mathrm{i}} + \Gamma_{\mathrm{a}} T + \frac{\Gamma_{\mathrm{b}}}{\exp(E_{\mathrm{LO}}/k_{\mathrm{B}}T) - 1}, \qquad (2)$$

where Γ_{i} is inhomogeneous part, and Γ_{a},Γ_{b} represent the corresponding coupling strengths with acoustic and longitudinal optical (LO) phonon, respectively. E_{LO} is the energy of LO phonon, and k_{B} is the Boltzmann constant. Experimental data and the fitted results are shown in Fig. 4. The solid circles are PL line width data of samples A and B, and corresponding solid lines are the results fitted by Eq. (2). Comparing the measured PL line width and the fitting curves, we can see that the model of exciton scattering with acoustic and LO phonons well describes the thermal dynamics involved in the ternary III–V compounds that have two V groups (As and P). However, the measured line width data at 300 K for the large-strained sample A deviates

from the exponential rule and become narrow, while the PL line width for sample B increases exponentially with the entire measured temperature range. The measured results of another large-strained MQW sample (6-pair $InAs_{0.43}P_{0.57}$(4.8 nm)/InP(7.8 nm)) also shows similar characteristics as sample A. To describe the phonon behavior at high temperature in the MQWs that have large strains, a more accurate model is needed because strain relaxation may occur at high temperature.

Table 1 lists the parameters derived by applying Eq. (2) to the line width data using the least-square fitting procedure. The fitted values of inhomogeneous part (Γ_i) for samples A and B are small and approximately equal, which reveal that the two samples are good epitaxied by the same GSMBE. The acoustic phonon scattering contributions to homogeneous broadening are also almost the same for the two structures. Furthermore, it is found that the parameters listed in Table 1 have the relation $(\Gamma_b)_A/(\Gamma_b)_B = (E_{LO})_A^{1/2}/(E_{LO})_B^{1/2}$, where subscripts at right corner represent samples A and B, respectively. Under the assumption that the high frequency and static frequency dielectric constants, the effective electron and hole masses are the same for the quantum wells in both samples, and the relation obtained has the same form as that deduced from the theory of exciton–longitudinal phonon coupling strength [21]. On the other hand, Γ_b for sample A is bigger than that for sample B. This may be attributed to the fact that LO phonon is localized in wells due to the different LO phonon dispersion relations of well layer and barrier layer materials [22]. The larger strain involved in the well layers of sample A is easier to relax at the interfaces of QWs. The breakdown of bonding at the interfaces may render the stronger localization of LO phonon. Thus, the fitted strength of excitons scattering with LO phonon is bigger in strained sample A than strain-compensated sample B.

Table 1
Parameters for fitting the temperature dependence of PL spectra line width

Sample	E_{LO}(meV)	Γ_i(meV)	Γ_a(meV/K)	Γ_b(meV)
A	36.1	7.22	0.030	17.1
B	33.5	9.16	0.032	16.5

Fig. 5 shows PL emission efficiency η as the function of temperature. Here the integrated intensity of PL spectra is normalized, i.e. the

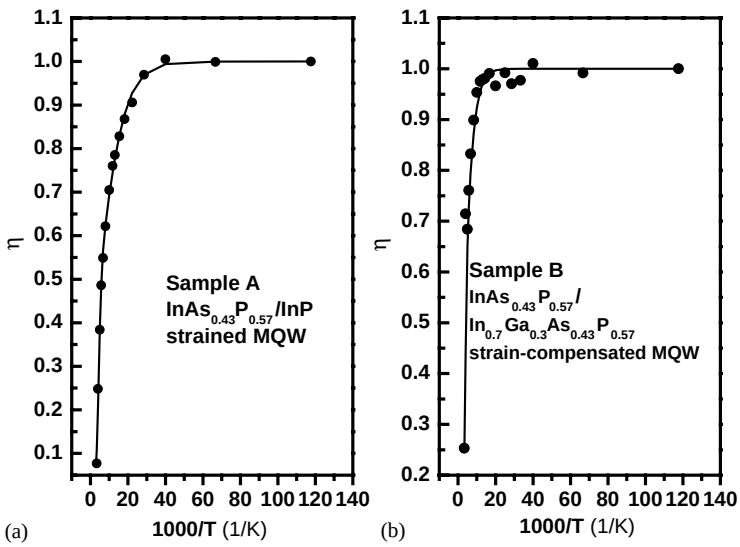

Fig. 5. Inverse temperature dependence of PL spectra emission efficiency η. The solid circles are normalized experiment data, and the solid curves are the results fitted by applying Eq. (3) to the measured data with a least-square fitting procedure. When temperature rises up to 50 K, the emission efficiency reduces to 90% for sample A, but 120 K for sample B.

integrated intensity of PL spectra at other temperature is divided by the maximum value at 8.5 K. The solid circles in Fig. 5(a) and (b) represent the normalized measured data of samples A and B, respectively. The behaviors of emission efficiency versus temperature can be characterized by two temperature ranges both of which obey Arrhenius dependence. They correspond to two thermally activated nonradiative recombination mechanisms and processes. The temperature dependence of PL emission efficiency $\eta(T)$ can be described by [23]

$$\eta(T) = 1/[1 + C_1 \exp(-E_1/k_B T) + C_2 \exp(-E_2/k_B T)], \quad (3)$$

where C_1, and C_2 are the ratios of thermally activated nonradiative recombination to excitonic radiative recombination probabilities for the two loss mechanisms. E_1, E_2 are corresponding thermal activation energies and k_B is the Boltzmann constant. Table 2 lists the parameters derived by applying Eq. (3) to the normalized data using a least-square fitting procedure. The PL emission efficiency in low-temperature range is mainly determined by $C_1\exp(-E_1/k_B T)$. In this temperature range, the thermal activation energy ($E_1 = 12.3$ meV) for sample A is much smaller than that for sample B ($E_1 = 31.6$ meV). The smaller thermal activation energy means that thermally activated nonradiative recombination can easily occur in sample A. As a result, η decreases to 90% when temperature rises up to 50 K for sample A, while it is 120 K for sample B.

Thermally activated nonradiative recombination in high-temperature range results from the thermal activation of carriers related to the transitions of high energy sub-bands [24], as it can be seen from the PL line shape changes versus temperature in Fig. 2. As temperature increases, PL spectra change from a symmetrical line shape to an asymmetrical line one, indicating the enhancement of electronic transitions of higher energy sub-bands due to thermal activation.

It is interesting to note from Fig. 5 that the PL emission efficiency only decays 4 times when temperature rises from 8 to 300 K for the strain-compensated sample B, while for the strained sample A it decays 10 times. The strain relaxation at high temperature for the strained MQW sample significantly degrades the luminescent efficiency. The above results indicate that strain-compensated InAsP/InGaAsP MQWs have better luminescent properties and weaker thermally activated nonradiative recombination processes involved than strained InAsP/InP MQWs.

Table 2
Parameters for fitting the inverse temperature dependence of PL spectra emission efficiency η

Sample	C_1	C_2	E_1 (meV)	E_2 (meV)
A	1.84	781.85	12.3	122.6
B	2.28	1201.57	31.6	162.2

4. Conclusions

Strained $InAs_{0.43}P_{0.57}$/InP MQW and strain-compensated $InAs_{0.43}P_{0.57}/In_{0.7}Ga_{0.3}As_{0.43}P_{0.57}$ MQW structures were grown by GSMBE. By low-temperature PL measurements, we have investigated the differences of the PL spectra of the two samples. The temperature dependence of the 1e–1hh transitions of the two quantum well structures is similar to that of corresponding bulk material. The temperature dependence of PL spectra line width and the characters of exciton–longitudinal phonon coupling strength of the two samples are studied and explained semi-quantitatively. The thermal activation energies in two temperature ranges are larger for strain-compensated MQW than for the strained one. As temperature increases the PL emission efficiency of both samples decreases. However, the PL emission efficiency of the strain-compensated MQW decays much slower than that of strained MQW. Thus the good temperature stability of luminescence efficiency in the strain-compensated sample is realized. The results obtained by PL studies can be applied to the design and fabrication of optoelectronic devices containing strained MQWs.

References

[1] H. Sugiura, J. Crystal Growth 164 (1996) 434.
[2] H. Sugiura, M. Ogasawara, M. Mitsuhara, M. Itoh, Y. Kondo, J. Crystal Growth 188 (1998) 260.

[3] C.Y. Lee, M.C. Wu, H.P. Shiao, T.T. Shi, W.J. Ho, Solid-State Electron. 43 (1999) 2141.
[4] J.P.R. David, M. Hopkinson, P.N. Stavrinou, S.K. Haywood, J. Appl. Phys. 78 (1995) 3330.
[5] P.J.A. Thijs, L.F. Tiemeijer, J.J.M. Binsma, T. Vandongen, Philips J. Res. 49 (1995) 187.
[6] H. Oohashi, S. Seki, T. Hirono, H. Sugiura, T. Amano, M. Ueki, J. Nakano, M. Yamamoto, Y. Tohmori, M. Fukuda, K. Yokoyama, Electron. Lett. 31 (1995) 556.
[7] Z.B. Hao, Z.Y. Ren, W. He, Y. Luo, Jpn. J. Appl. Phys. Part 1 41 (2002) 754.
[8] H.Y. Chung, G. Stareev, J. Joos, M. Golling, J. Mahnss, K. Ebeling, J. Crystal Growth 202 (1999) 909.
[9] J.X. Chen, A.Z. Li, Y.Q. Chen, Y.G. Zhang, M. Qi, X.R. Lin, K. Frojdh, B. Stoltz, Compound Semiconductor 166 (2000) 63.
[10] Matsuyuki Ogasawara, Hideo Sugiura, Manabu Mitsuhara, Mitsuo Yamamoto, Masashi Nakao, J. Appl. Phys. 84 (1998) 4775.
[11] S.L. Chuang, Phys. Rev. B 43 (1991) 9649.
[12] Y.Q. Chen, A.Z. Li, J. Crystal Growth 227 (2001) 1171.
[13] T. Schmidt, K. Lischka, W. Zulehner, Phys. Rev. B 45 (1992) 8989.
[14] Y. Varshni, Physica 34 (1967) 149.
[15] S. Tiwari, Compound Semiconductor Device Physics, Academic Press, New York, 1992.
[16] V. Wilkinson, A. Adams, in: P. Bhattacharya (Ed.), Properties of Lattice-Matched and Strained Indium Gallium Arsenide in EMIS Datareviews Series, Vol. 8, IEE INSPEC, 1993, p. 77 (Section 3.2).
[17] A. Katz, Indium Phosphide and Related Materials, Artech House, Boston, 1992.
[18] J. Singh, Physics of Semiconductors and their Heterostructures, McGraw-Hill, New York, 1993.
[19] L.M. Woods, P. Silvestre, P. Thiagarajan, G.A. Patrizi, G.Y. Robinson, K.M. Jones, M.AL. Jassim, J. Electron. Mater. 23 (1994) 1229.
[20] A. Venu Gopal, Rajesh Kumar, A.S. Venguriekar, A. Bosacchi, S. Franchi, L.N. Pfeiffer, J. Appl. Phys. 87 (2000) 1858.
[21] W.Z. Shen, Appl. Phys. Lett. 79 (2001) 1285.
[22] X.C. Shen, Spectroscopy and Optical Properties in Semiconductor, 2nd ed., Science Press, Beijing, 2002.
[23] J.D. Lambkin, L. Considine, S. Walsh, G.M. O'Connor, C.J. McDonagh, T.J. Glynn, Appl. Phys. Lett. 65 (1994) 73.
[24] W.Z. Shen, S.C. Shen, W.G. Tang, Y. Chang, Y. Zhao, A.Z. Li, J. Phys.: Condens. Matter. 8 (1996) 4751.